Structure of D-glyceraldehyde-3-phosphate dehydrogenase from *Palinurus versicolor* in a tetragonal crystal form

SHEN Yuequan (沈月全), SONG Shiying (宋时英) & LIN Zhengjiong (林政炯)

National Laboratory of Biomacromolecules, Institute of Biophysics, Chinese Academy of Sciences, Beijing 100101, China
Correspondence should be addressed to Lin Zhengjiong (email: lin@suns.ibp.ac.cn)

Received May 19, 1999

Abstract D-glyceraldehyde-3-phosphate dehydrogenase (holo-GAPDH) from *Palinurus versicolor* was crystallized in a novel crystal form by the method of sitting-drop vapor diffusion. The crystals have space group $P42_12$, cell parameters a=15.49 nm, c=8.03 nm and two subunits per asymmetric unit. The crystal structure at 0.34 nm was determined by the molecular replacement method. The final model has crystallographic R_{free} and R factors of 0.274 and 0.262, and r.m.s. deviations of 0.002 nm for bond lengths and 2.33° for bond angles. The two subunits in asymmetric unit are similar to each other not only in the three-dimensional structure, but also in average temperature factors. This result demonstrates that the obvious difference in average temperature factors for the different subunits in $C2$ crystal form reported previously may be attributed to the different crystallographic environments of the subunits. This further supports that holo-GAPDH has a good 222 molecular symmetry.

Keywords: D-glyceraldehyde-3-phosphate dehydrogenase, allosteric enzyme and crystal structure.

Glycolytic D-glyceraldehyde-3-phosphate dehydrogenase (GAPDH: EC 1.2.1.12) is tetrameric enzyme which catalyzes the oxidative phosphorylation of D-glyceraldehyde-3-phosphate to form 1,3-diphosphoglycerate in the presence of NAD^+ and inorganic phosphate. GAPDH has four chemically identical subunits. Every subunit includes 333 residues. The molecular weight of GAPDH tetramer is about 145 ku.

GAPDH is an allosteric enzyme, which can show various cooperative properties for binding coenzyme depending on its sources. GAPDH in yeast manifests positive cooperativity and in muscle shows negative cooperativity. Especially when reacting with certain acylating reagents, GAPDH exhibits half-of-the-sites property[1]. Therefore, GAPDH is a good model for researching allosteric mechanism.

Several high-resolution GAPDH structures have been published[2−5]. It is important to know whether the four subunits are identical or not in order to discern the type of allosteric model. All known GAPDH structures including that from PV reveal good 222 molecular symmetry, in other words, the four subunits are identical. In high-resolution structures of PV GAPDHases (holo-GAPDH, CM-GAPDH) in $C2$ crystal form, the average B factors differ significantly

Abbreviations: GAPDH, D-glyceraldehyde-3-phosphate dehydrogenase; holo-GAPDH, NAD^+-saturated GAPDH; CM-GAPDH, active-site carboxymethylated GAPDH; r.m.s., root-mean-square; PV, *Palinurus versicolor*.

between the two subunits in the asymmetric unit, especially for holo-GAPDH. Is the *B* factor difference induced by different crystallographic environment or is it just a reflection of inherent molecular asymmetry? The structure in a new crystal form may clarify this question and help improve understanding of the flexibility of the enzyme. Crystal growth of novel crystal form ($P42_12$), structure determination with molecular replacement, structure description and comparison of the structures in different crystal forms are reported in this paper.

1 Experiments

1.1 Crystal growth

According to the method of Allison and Kaplan[6], PV holo-GAPDH was purified from the tail muscle of lobster in Chinese South Sea. The crystals were grown by sitting-drop vapor diffusion in 20 μL inner-drop containing 5 mg/mL holo-GAPDH, 1 mmol/L EDTA, 1.6 mol/L $(NH_4)_2SO_4$, 0.2 mol/L potassium phosphate buffer (pH 6.2) and 6 mL outer-drop containing 2.7 mol/L $(NH_4)_2SO_4$, 0.2 mol/L potassium phosphate buffer (pH 6.2). The crystallization conditions were similar to those described by Song et al.[7] except that NAD^+ molecules were not added. In *C*2 crystal form, 0.5 mmol/L NAD^+ molecules were added. This vapor diffusion system was put into the constant-temperature box (18 ℃). Crystals appeared in four days and were harvested in two weeks. The crystals are of rectangle prism shape with the longest dimension of 0.6 mm (fig. 1). The crystal can diffract to higher than 0.34 nm resolution.

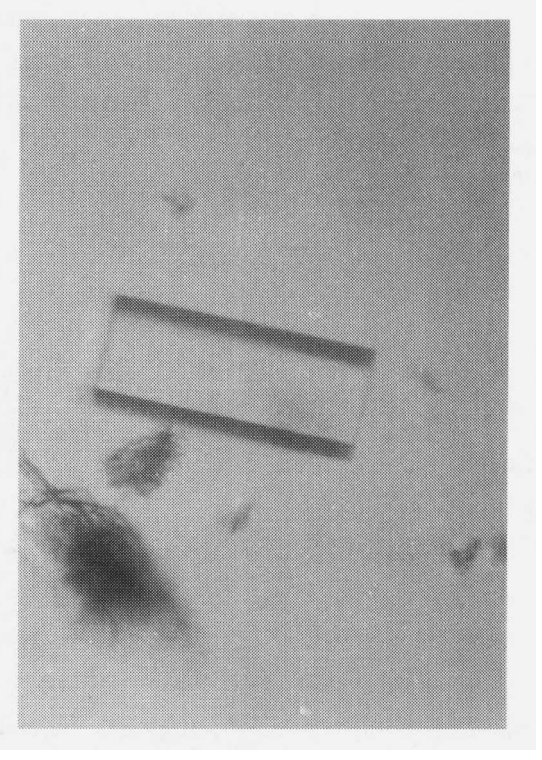

Fig. 1. The tetragonal crystal of holo-GAPDH.

1.2 Data collection, processing and molecular replacement solution

The data were collected with Mar Research Image Plate system and processed using the software, Denzo and Scalepack[8]. Data analysis showed that the space group is $P42_12$ with cell parameters a=15.49 nm, c=8.03 nm. It was estimated that there were two subunits per asymmetric unit[9]. The data set has R_{merge} of 15.2% and average redundancy of 4 and contains 12 829 unique reflections with completeness of 91.4% for all data (>0.34 nm) and 83.9% for the outer-shell (0.34—0.35 nm).

Molecular replacement was performed using the program AMoRe[10]. The search model was the green subunit of PV holo-GAPDH in *C*2 crystal form (NAD^+ and water molecules were excluded). The rotation function was calculated using the data in the resolution range of 0.8—0.4 nm with an integration radius of 2 nm. The cross-rotation search showed that the top two peaks of the rotation function appeared with correlation values of 16.7 and 14.0. One-body and two-body translation functions confirmed that these two rotation search peaks were correct by the significance of the correlation coefficients, and yielded the correct molecular position information. The rigid-body refinement of AMoRe resulted in an *R* factor of 25.7% and a correlation value of 81.9% (table 1). The initial model, oriented and positioned according to the molecular replacement solution, was examined with the program TURBO-FRODO[11] and confirmed that the molecular packing in the crystal lattice was reasonable.

Table 1 The result of molecular replacement

Cross-rotation								
No.	α		β	γ	Corr.			
A	43.50		23.80	1.99	16.7 (13.7)			
B	45.28		23.18	179.13	14.0 (13.7)			
Translation								
	No.		x	y	z		Corr.	R
$P42_12$	A		0.116	0.812	0.221		40.3 (23.3)	45.8 (51.0)
	B		0.370	0.798	0.076		76.3 (24.3)	29.5 (50.6)
Fiting								
No.	α	β	γ	x	y	z	Corr.	R
A	45.10	23.97	−0.46	0.117	0.812	0.219	81.9	25.7
B	45.95	23.74	179.64	0.369	0.798	0.075	81.9	25.7

A and B, solution label; Corr., correlate coefficient; α, β and γ, eularian angle; x, y and z, fraction coordinate. The highest noise peak value is in brackets.

1.3 Structure refinement

The refinement was carried out using the X-PLOR[12] with imposing non-crystallographic symmetry restraints. The first step was based on rigid-body least-squares refinement with an initial model in the resolution range 1.0—0.4 nm ($F>2\sigma$). The R_{free} value decreased to 0.292 after 40 successive cycles. The electron density of NAD^+ molecules, which were not included in search model, was clearly shown (fig. 2). The resolution range was then extended to 0.34 nm. Refinement was followed by a combination of positional refinement, simulated annealing and group *B*-factor refinement. $2F_o$-F_c and F_o-F_c maps were calculated and examined to adjust the side-chains of some residues. NAD^+ molecules and sulfate ions were identified by their bulk electron density. Water molecules were gradually included in the model. They were positioned only when well-defined positive peaks appeared in both the $2F_o$-F_c and F_o-F_c difference maps and when they could form hydrogen bonds either with protein atoms or other water molecules.

2 Results

2.1 Model quality

The final model containing 5 012 non-hydrogen protein atoms, two NAD^+ molecules, four SO_4^{2-} ions and sixteen water molecules, gives an R_{free} of 0.274 and *R* factor of 0.262 for reflections

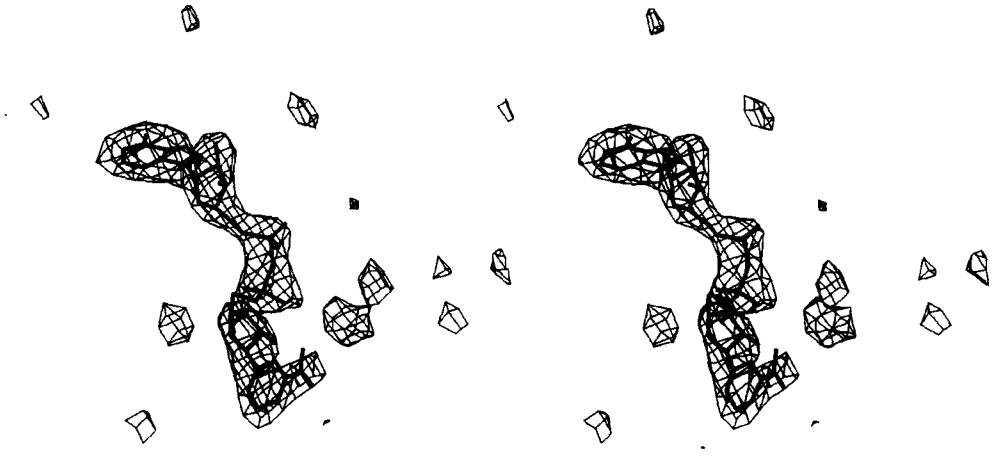

Fig. 2. The electron density map of NAD^+ molecule in the monomer.

in the resolution range of 1.0—0.34 nm and r.m.s. deviations from ideal stereo-chemistry of 0.002 nm for bond lengths, 2.33° for bond angles. The model has a good electron density and reasonable Ramanchandran diagram. These results demonstrate that the structure of holo-GAPDH in $P42_12$ crystal form is reliable. In order to check the difference in *B* factors of different subunits, the refinement was carried out without imposing non-crystallographic restraints. The result displayed that the average *B* factors of two subunits in asymmetric unit do not have significant difference (0.32 nm^2 for the green subunit and 0.38 nm^2 for the red subunit). In discussing issue concerning *B* factors (see below), the model without imposing non-crystallographic symmetry restraints during refinement was used.

2.2 Structure comparison with *C*2 crystal form

2.2.1 Monomer. GAPDH consists of four identical subunits: red, green, blue and yellow[13]. In the high-resolution structure of *C*2 crystal form, the two subunits (red, green) in asymmetric unit reveal good non-crystallographic two-fold symmetry and the r.m.s. deviations of Cα atoms for the two subunits are only 0.0199 nm. In the structure of $P42_12$ crystal form, the two subunits (red, green) in asymmetric unit are not distinguishable. Therefore, only one subunit (green) was used in the structure comparison of two crystal forms.

The superposition of Cα atoms of single subunit in the two crystal forms (fig. 3) gives r.m.s. deviations of 0.0332 nm for catalytic domain, 0.0456 nm for NAD^+-binding domain and 0.0411 nm for the whole subunit. These data demonstrate that the subunit structures in the two crystal forms are similar to each other. The r.m.s. deviations of Cα atoms of every residue against residue number are plotted in fig. 4. The residues having large r.m.s. deviations are Lys191 (0.090 nm) and Asp192 (0.088 nm) in catalytic domain and Glu21 (0.100 nm), Gly55 (0.080 nm), Asp61 (0.122 nm), Gly62 (0.070 nm), Ser333 (0.212 nm) and Ala334 (0.227 nm) in NAD^+-binding

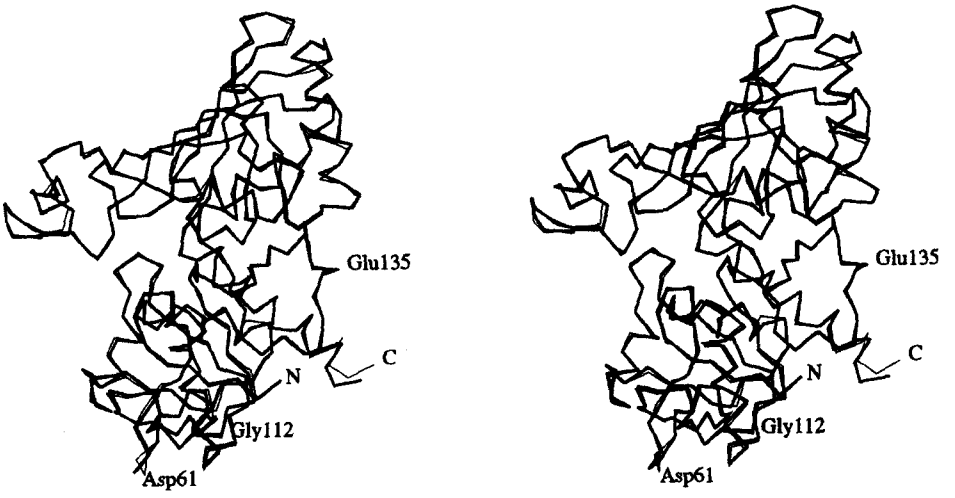

Fig. 3. The superposition plot of Cα atoms of the green subunit between two crystal forms: thin line, *C*2; thick line, $P42_12$.

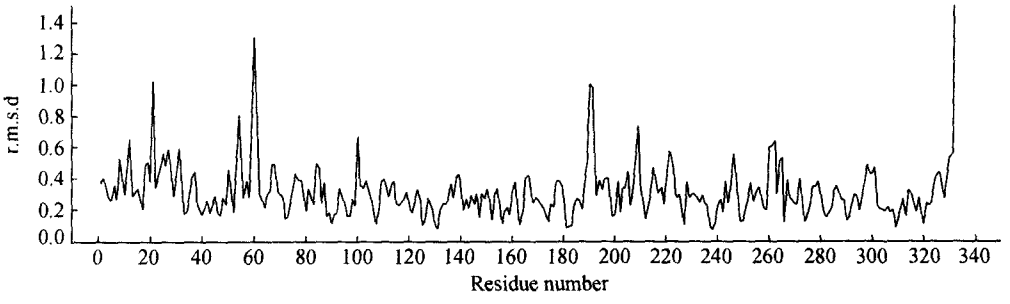

Fig. 4. The r.m.s. deviations of Cα atoms between GAPDH molecules in $P42_12$ and *C*2 along the polypeptide chain (the green subunit).

domain. In *C*2 crystal form, Asp61 having poor electron density is located on molecular surface. While in $P42_12$ crystal form, this residue makes a hydrogen bond with residue Lys2 from neighboring tetramer. The structure differences led to the change in the location of Gly62. In the two crystal forms, residues Glu21, Gly55, Lys191 and Asp192 are located on the surface of molecule and near to solvent region, thus, are flexible. Ser333 and Ala334 at C-end are also flexible. Even in *C*2 crystal structure at 0.2 nm resolution, they do not have well defined electron density. If these two residues are deleted in the calculation, the Cα r.m.s. deviations will decrease to 0.036 nm for the whole subunit and 0.038 nm for NAD^+-binding domain.

In both crystal forms, NAD^+ molecules occupy identical positions indicating that crystal packing does not have effect on the binding of NAD^+ molecule. In $P42_12$ crystal form, the occupancy of NAD^+ molecule is about 85%. This may be related to the conditions of crystal growth, NAD^+ were not added in the crystallization solution.

2.2.2 Tetramer. High-resolution GAPDH structures from various species show that the enzyme molecule has good 222 symmetry. In *C*2 and $P42_12$ crystal forms of PV GAPDH, molecular Q

axis coincides with crystallographic two-fold axis. The two subunits in asymmetric unit are related by a non-crystallographic symmetry axis, which coincides with R axis. The nomenclature of molecular axes (P, Q, R) is the same as that in *Homarus americanus* GAPDH structure[13].

Tetrameric structures in both crystal forms are also similar. The superposition of the two tetramers gives Cα r.m.s. deviations of 0.046 nm. Furthermore, in the two crystal forms, no significant differences in salt bonds and hydrogen bonds in the interfaces were found. The solvent structure in the interface could not be found because of the low-resolution of the structure.

From the similarity in overall structure and inter-subunit interactions, it can be inferred that solvent structures within subunit and in the inter-subunit interfaces may be similar in both crystal forms. As an example, SO_4^{2-} ions in both crystal forms occupy similar positions. Although the occupancy of SO_4^{2-} is only 60% in $P42_12$ crystal form, its position could be discerned from $2F_o$-F_c and F_o-F_c electron density map.

2.2.3 Crystal packing. The crystal packing is dissimilar in two crystal forms. Each tetramer has six neighbors and the unique interactions between tetramers are listed in table 2. Fig. 5 (a), (b) shows the packing of GAPDH molecules in the two crystal forms as viewed down along the *c* axis. In fig. 5, reference tetramer sym0 and four neighboring tetramers (sym1, sym2, sym3, sym4) are located in the same *ab* plane and another two neighboring tetramers (sym5, sym6) created by the symmetry operations (0, 0, −1) and (0, 0, 1), are not displayed.

Table 2 The comparison of the inter-tetrameric interactions

$P42_12$			$C2$		
Atom 1 sym0	Atom 2 sym2	Dist /nm	Atom 1 sym0	Atom 2 sym2	Dist/nm
G-OD2-Asp254	R-NZ-Lys159	0.312	G-OE2-Glu135	R-OE1-Glu135	0.340
G-O-Glu249	R-OE2-Glu163	0.279	G-OE2-Glu135	R-OE2-Glu135	0.290
G-Asn164	R-Pro266	vdw	G-O-Glu135	R-NZ-Lys136	0.309
G-Lys248	R-Asn164	vdw	G-Lys136	R-Glu135	vdw
G-Asp253	R-Glu135	vdw	G-Glu163	R-Pro266	vdw
G-Ala257	R-Pro266	vdw	G-Glu163	R-Gly265	vdw
G-Ala257	R-Gly265	vdw	G-Gly265	R-Glu163	vdw
G-Ala261	R-Gly265	vdw	G-Pro266	R-Glu163	vdw
sym0	sym1		G-NE2-Gln268	R-O-Glu163	0.328
G-OD1-Asp61	R-NZ-Lys2	0.349	sym0	sym6	
sym0	sym6		G-OE1-Glu103	B-OE1-Glu103	0.338
G-Phe109	B-Phe109	vdw	G-Ile102	B-Lys110	vdw
G-Lys110	B-Lys142	vdw	G-Lys110	B-Lys142	vdw

G, The green subunit; R, the red subunit; B, the blue subunit; vdw, Van der Waal force. sym0, a GAPDH tetramer; sym1, sym2 and sym6, the labels of tetramers which are in contact with sym0. See fig. 5, sec. 2.2.3. The contact distance is less than 0.35 nm.

In *C*2 crystal form, *Q* axis coincides with crystallographic *b* axis and *P* axis with *a* axis and intersects projection plane at an angular of about 25° (fig. 5 (b)). While, in $P42_12$ crystal form, *Q* axis of tetramer coincides with crystallographic *a*+*b* axis, and *P* axis intersects *ab* plane at 25° (fig. 5(a)). Therefore, figs. 5(a) and 5(b) reveal similar tetramer view. In $P42_12$ crystal form, the

tetramers located on *ab* plane and in contact with sym0 were rotated by 90° along *c* axis in comparison with *C*2 crystal form.

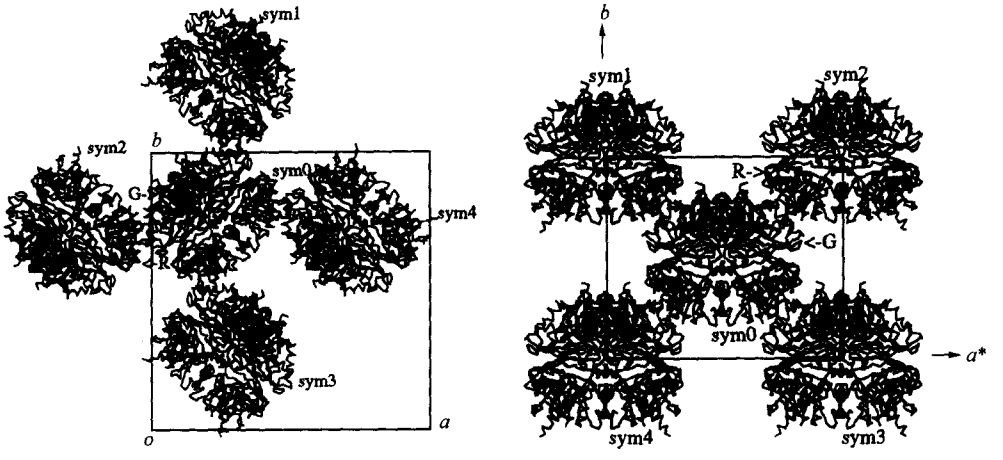

Fig. 5. The crystal packing in two crystal forms (viewed down along *c* axis): (a) $P42_12$ crystal form; (b) *C*2 crystal form.

In *C*2 crystal form, the contact region in the *ab* plane involves the same region of the green and red subunits. This region consists of turn (Gly265-Gly269) and α-helix (Ser148-Glu166) in catalytic domain and loop (Glu135-Lys136) in NAD^+-binding domain. Residues taking part in the interactions at this region are related by a non-crystallographic two-fold axis, which parallels the *R* axis. This region could be found in the red subunit of $P42_12$ crystal form, but not in the green subunit where a similar region consists of turn (Leu246-Cys250) and helix (Ser251-Glu264). An additional contact region consisting of Asp61 of the green subunit and Lys2 of the red subunit was observed in $P42_12$ crystal form. This region is absent in *C*2 crystal form. In the two crystal forms, a contact region, which consists of α-helix (Thr101-Gly112) of NAD^+-binding domain of the green subunit and β-sheet (Lys142-Asn146) and α-helix (Thr101-Gly112) of the blue subunit, connects two tetramers translated along *c* axis.

The numbers of intertetrameric interactions are similar in the two crystal forms. However, interactions are different in respect to the domain distribution (see table 2). In *C*2 crystal form, there are twelve interactions in total. Among those, seven occur between NAD^+-binding domains of two tetramers and five between catalytic domains. However, in $P42_12$ crystal form, there are eleven interactions in total. Among them, three occur between NAD^+-binding domains, seven between catalytic domains and one between NAD^+-binding domain from one tetramer and catalytic domain from another.

3 Discussion

The tetragonal crystal diffracts to only 0.34 nm. In order to improve the ratio of data to

parameters, the RESTRAIN non-crystallographic restraints were applied in structure refinement. High-resolution X-ray crystallographic studies demonstrate that the monomeric structures of GAPDH are remarkably similar to each other. The structural differences are within experimental errors[2−5]. Therefore, it is reasonable to apply the non-crystallographic restraints. As a matter of fact, the structure has better quality after refinement.

Structural comparison reveals that both monomer and tetramer of the two crystal forms are very similar. Differences in crystal packing led to the differences in inter-tetrameric contact regions. However, no obvious structural changes were found for these contact sites, indicating less flexibility of GAPDH structure, which is hardly affected by the crystal packing force.

Owing to the differences in crystal packing, there are significant differences in inter-tetrameric interactions between the two crystal forms. Therefore, an important problem arising from the analysis of *C*2 GAPDH structure can be studied in detail. The problem is that the large difference between average *B* factors of subunits in *C*2 crystal form is induced by crystal packing or by inherent molecular asymmetry. Now, in the new crystal form, the two subunits in the asymmetric unit have similar average *B* factors, suggesting that the difference in average *B* factor observed in *C*2 crystal form is induced by crystal packing. In the green subunit of the two crystal forms, the inter-tetrameric interactions are distributed over two distant contact sites, stabilizing the subunit and resulting in lower average *B* factor. In the red subunit of *C*2 crystal form, the inter-tetrameric interactions are involved in only one contact region for NAD^+-binding domain. This region consists of Glu135 and Lys136, being located on the waist of monomer. In $P42_12$ crystal form, besides Glu135 contact region, another contact region consisting of Lys2 joins the inter-tetrameric interaction of the red subunit, where Lys2 is far from Glu135. This difference makes NAD^+-binding domain of the red subunit less flexible in $P42_12$ crystal form than in *C*2 crystal form. This explains the average *B* factor difference in *C*2 crystal form (0.29 nm^2 and 0.53 nm^2) and similarity in $P42_12$ crystal form (0.33 nm^2 and 0.37 nm^2). Therefore, the difference of average *B* factor of two subunits in *C*2 crystal form does not suggest the inherent molecular asymmetry, indicating that the tetramer of GAPDH has good 222 molecular symmetry indeed. For this reason, it is reasonable to explain the negative-cooperativity mechanism by ligand-induced model. Further studies on negative-cooperativity of GAPDH are underway.

Acknowledgements The authors thank Prof. Tsou Chenlu for his most valuable suggestions and Prof. Zhou Junmei for her most helpful discussion in purification. This work was supported by the National Natural Science Foundation of China (Grant Nos.39370164, 39570169).

Reference

1. Levitzki, A., Half-of-the-sites and all-of-the-sites reactivity in rabbit muscle glyceraldehyde-3-phosphate dehydrogenase, J. Mol. Biol., 1974, 90: 451.
2. Song, S. Y., Li, J., Lin, Z. J., Structure of holo-glyceraldehyde-3-phosphate dehydrogenase from *Palinurus versicolor* refined at 2.0 resolution, Acta Cryst., Ser. D, 1998, 54(4): 558.
3. Skarzynski, T., Moody, P. C. E., Wonacott, A. J., Structure of holo-glyceraldehyde-3-phosphate dehydrogenase from *Bacillus stearothermophilus* at 1.8Å resolution, J. Mol. Biol., 1987, 193: 171.

4. Korndorfer, I., Steipe, B., Huber, R. et al., The crystal structure of holo-glyceraldehyde-3-phosphate dehydrogenase from the hyper-thermophilic bacterium *Thermotoga maritima*, J. Mol. Biol., 1995, 246: 511.
5. Emile, D., Olivier-Deyris, L., Fanchon, E. et al., Comparison of the structures of wild-type and a N313T mutant of *Escherichia coli* glyceraldehyde–3-phosphate dehydrogenase: implication for NAD binding and cooperativity, J. Mol. Biol., 1996, 257: 814.
6. Allison, W. S., Kaplan, N. O., The comparative enzymology of triosephosphate dehydrogenase, J. Biol. Chem., 1964, 239(7): 2140.
7. Song, S. Y., Gao, Y. G., Xie, G. F. et al., Preliminary crystallographic studies of the coenzyme binding to D-glyceraldehyde–3-phosphate dehydrogenase from *Palinurus versicolor*, Science in China, Ser. B, 1988, 31(2): 139.
8. Otwinowski, Z., Minor, W., Processing X-ray diffraction data collected in oscillation mode, Methods Enzymol., 1997, 276: 307.
9. Matthews, B.W., Solvent content of protein crystals, J. Mol. Biol., 1968, 33: 491.
10. Navaza, J., AmoRe: an automated package for molecular replacement, Acta Cryst. Sect. A, 1994, 50(4): 760.
11. Roussel, A., Cambillau, C., TURBO-FRODO, in Silicon Graphics Geometry Partners Directory, CA: Silicon Graphics, Mountain View, 1989, 77—78.
12. Brunger, A.T., XPLOR Manual, Version 3.1, New Haven: Yale University, 1992.
13. Buehner, M., Ford, G. C., Moras, D. et al., Three-dimensional structure of D-Glyceradehyde-3-phosphate dehydrogenase, J. Mol. Biol., 1974, 90: 25.